Structural Diversity and Magnetic Properties of Two Coordination Polymers Based on 6-(3,5-Dicarboxylphenyl)nicotinic Acid①

ZHAI Li-Jun[a, c] TONG Ru[a] WANG Ci-Bin[a] SHI Meng-Jie[a]
MO Ya-Nan[a] CHE Wen-Kai[a] NIU Yu-Lan[a②] HU Tuo-Ping[b②]

[a] (*Taiyuan Institute of Technology, Department of Chemistry and Chemical Engineering, Taiyuan* 030008, *China*)
[b] (*Department of Chemistry, College of Science,North University of China, Taiyuan* 030051, *China*)
[c] (*Key Laboratory of Advanced Energy Materials Chemistry* (*Ministry of Education*), *College of Chemistry, Nankai University, Tianjin* 300071, *China*)

ABSTRACT Two new coordination polymers, namely $\{[Co_8(DCPN)_4(1,2\text{-bimb})_4(\mu_3\text{-OH})_4]\cdot(CH_3CN)_{0.5}(H_2O)_2\}_n$ (**1**) and $\{[Co_2(DCPN)(1,3\text{-bimb})(\mu_3\text{-OH})]\cdot H_2O\}_n$ (**2**), where H_3DCPN = 6-(3,5-dicarboxyl-phenyl)nicotinic acid, 1,2-bimb = 1,2-bis(imidazole-1-methyl)benzene and 1,3-bimb = 1,3-bis(imidazole-1-methyl)benzene, have been solvothermally synthesized and structurally characterized by single-crystal X-ray diffraction analysis, elemental analysis (EA), infrared (IR) analysis, powder X-ray diffraction (PXRD) and thermogravimetric analysis (TGA). The structural analysis indicated that **1** is a 2D structure based on two different $[Co_4(DCPN)_2(\mu_3\text{-OH})_2]_n$ SBUs, and **2** is a 3D framework based on $[Co_4(DCPN)_2(\mu_3\text{-OH})_2]$ SBUs. In addition, the magnetic measurements showed that **1** and **2** have antiferromagnetic interactions between adjacent Co(II) ions. The slight difference of magnetic properties between **1** and **2** may be attributed to their different structures formed during the assembly process.

Keywords: coordination polymers, solvothermal synthesis, magnetic properties;
DOI: 10.14102/j.cnki.0254-5861.2011-3354

1 INTRODUCTION

As a new class of organic-inorganic hybrid materials, coordination polymers (CPs) with adjustable structure and high specific surface area[1-3] have a wide range of potential applications in gas adsorption and separation[4, 5], fluorescence[6, 7], catalysis[8, 9], magnetism[10-13], etc. Among them, the magnetic properties of CPs have become one of the hot spots, which largely depends on the choice of central metal ions and ligands. According to the literature[14], by the incorporation of magnetic moment carrier (magnetic metal node or connector) into CPs in the self-assembly process, the magnetic CPs with different SBUs can be synthesized, and the existence of different SBUs endows the CPs with good stability and strong antiferromagnetic interaction. Currently, transition metals such as Cu, Mn, Fe, Co and Ni are usually used as magnetic metal centers[15-21]. As for ligands, aromatic polycarboxylic acids are one of the preferred bridging ligands to construct CPs based on the following two aspects: (a) its carboxylate groups can adopt a variety of coordination modes to construct versatile CPs with different SBUs; (b) its rigidity helps to build CPs with stable structure.

Inspired by the above considerations, based on a N-containing 6-(3,5-dicarboxylphenyl)nicotinic acid (H_3DCPN), 1,2-bis(imidazole-1-methyl) benzene (1,2-bimb), 1,3-bis-(imidazole-1-methyl) benzene(1,3-bimb) and cobalt salts, two new CPs, **1** and **2,** were successfully obtained under solvothermal conditions. Meanwhile, the phase purity and

Received 6 September 2021; accepted 8 November 2021 (**CCDC 2067601 for 1 and 2067600 for 2**)

① Supported by the NSF of China (No. 21676258), the Scientific and Technologial Innovation Project of Shanxi Province (No. 2020L0647), Innovation and Entrepreneurship Project of Taiyuan Institute of Technology (No. S202114101015), and Open Foundation of Key Laboratory of Advanced Energy Materials Chemistry, Ministry of Education, Nankai University

② Corresponding authors. Prof. Niu Yu-Lan (1970-), majoring in coordination chemistry. E-mail: niuyl@tit.edu.cn;
Prof. Hu Tuo-Ping (1969-), majoring in inorganic chemistry. E-mail: hutuoping@nuc.edu.cn

structural stability of CPs were characterized by powder X-ray diffraction (PXRD) and thermogravimetric analysis (TGA), respectively. In addition, the magnetic susceptibilities (χ_M) of **1** and **2** were studied under the external 1000 Oe field in the temperature range of 2~300 K.

2 EXPERIMENTAL

2. 1 Materials and measurements

All analytical chemicals and reagents were received from commercial sources and used without further purification. C, H, and N analyses were made on a Vario EL analyzer. The crystal structures were performed on a Bruker Apex II CCD diffractometer. The thermogravimetric analyses were determined on a ZCT-A analyzer at a heating rate of 10 ℃·min^{-1} under air atmosphere. The IR spectra were recorded on a FTIR-8400s spectrometer with KBr discs in the 4000~400 cm^{-1} region. The magnetic properties of complexes **1** and **2** were measured with the Quantum Design SQUID MPMS XL-7.

2. 2 Syntheses of coordination polymers

2. 2. 1 Synthesis of {[Co_8(DCPN)$_4$(1,2-bimb)$_4$(μ_3-OH)$_4$] · ($CH_3CN)_{0.5}(H_2O)_2$}$_n$ (1)

A mixture of H_3DCPN (0.01 mmol, 2.9 mg), 1,2-bimb (0.02 mmol, 4.8 mg), $CoCl_2$ $6H_2O$ (0.02 mmol, 4.8 mg) and a mixed solution of DMA and H_2O (1 mL, V/V = 1/2) was sealed to a glass tube, which was heated at 120 ℃ for 72 h, then cooled to room temperature with a cooling rate of 1.4 ℃/h. The prune crystals of **1** were obtained with the yield of 48% (based on H_3DCPN). Anal. Calcd. (%) for $C_{113}H_{89.5}Co_8N_{20.5}O_{30}$: C, 50.48; H, 3.33; N, 10.69. Found (%): C, 50.51; H, 3.28; N, 10.73. IR (KBr pellet, cm^{-1}): 3458 (s), 1627 (s), 1606 (m), 1529 (m), 1440 (m), 1379 (w), 1059 (m), 861 (m), 773 (m), 691 (w), 492 (w) (Fig. S1).

2. 2. 2 Synthesis of {[Co_2(DCPN)(1,3-bimb)(μ_3-OH)] · H_2O}$_n$ (2)

The synthesis procedure of **2** is the same as that of **1** except that the 1,2-bimb was replaced by 1,3-bimb. The pink crystals of **2** were collected by washing with distilled water, filtering and drying in the air, with a yield of 55% (based on H_3DCPN). Anal. Calcd. (%) for $C_{28}H_{23}Co_2N_5O_8$: C, 49.75; H, 3.41; N, 10.36. Found (%): C, 49.78; H, 3.36; N, 10.32. IR (KBr pellet, cm^{-1}): 3457 (s), 1621 (m), 1590 (m), 1533 (m), 1436 (m), 1376 (m), 1043 (w), 833 (m), 765 (m), 644 (w), 544 (w) (Fig. S2).

2. 3 X-ray crystallography

The crystal data were gained with a Siemens SMART diffractometer using Mo-$K\alpha$ radiation (λ = 0.71073 Å) at 25 ℃. The structures of **1** and **2** were solved by direct methods with the non-hydrogen atoms refined anisotropically using the OLEX with F^2 value-based full-matrix least-squares method[22]. All the hydrogen atoms except those for water molecules were generated geometrically with fixed isotropic thermal parameters, and are included in the calculation of structure factors. Relevant crystallographic data, selected bond lengths and bond angles are shown in Table 1 and Table 2, respectively. Topological analysis was carried out by TOPOs program[23, 24].

Table 1. Crystallographic Data for 1 and 2

CPs	CP **1**	CP **2**
Empirical formula	$C_{113}H_{89.5}Co_8N_{20.5}O_{30}$	$C_{28}H_{23}Co_2N_5O_8$
Formula weight	2685.99	675.37
Crystal system	Triclinic	Monoclinic
Space group	$P\bar{1}$	$P2_1/n$
a (Å)	11.1352(13)	12.2216(19)
b (Å)	12.0992(14)	11.0562(17)
c (Å)	21.300(3)	21.653(3)
α (°)	102.8450(10)	90
β (°)	95.7680(10)	100.384(10)
γ (°)	99.8430(10)	90
Volume (Å^3)	2727.9(6)	2877.9(8)
Z	1	4
D_c (g cm^{-3})	1.635	1.599
μ (mm^{-1})	1.276	1.211
F(000)	1367.0	1376.0
Reflections collected	31266	23601
Independent reflections	12354	6621
Goodness-of-fit	1.001	1.033
R ($I > 2\sigma(I)$)	0.0475	0.0416
wR ($I > 2\sigma(I)$)	0.0996	0.0784

Table 2. Selected Bond Lengths (Å) and Bond Angles (°) of 1 and 2

CP **1**

Bond	Dist.	Bond	Dist.	Bond	Dist.
Co(1)–O(9)^1	2.140(2)	Co(2)–O(13)^3	2.261(3)	Co(3)–O(5)	2.160(2)
Co(1)–O(10)	2.075(2)	Co(2)–O(14)	1.974(2)	Co(3)–N(6)	2.134(3)
Co(1)–O(13)^1	2.088(2)	Co(2)–N(3)	2.066(4)	Co(4)–O(3)^1	2.265(2)
Co(1)–O(14)	2.076(2)	Co(3)–O(1)	2.063(2)	Co(4)–O(4)	1.967(2)
Co(1)–O(14)^2	2.117(2)	Co(3)–O(3)^1	2.094(2)	Co(4)–O(6)	1.985(2)
Co(1)–N(2)	2.111(3)	Co(3)–O(4)^4	2.084(2)	Co(4)–O(7)^4	2.005(2)
Co(2)–O(8)^3	1.990(2)	Co(3)–O(4)	2.112(2)	Co(4)–N(8)^4	2.066(3)
Co(2)–O(11)	1.982(2)				
Angle	(°)	Angle	(°)	Angle	(°)
O(10)–Co(1)–O(9)^1	85.22(9)	O(11)–Co(2)–O(8)^3	137.06(10)	O(4)^4–Co(3)–O(4)	79.35(9)
O(10)–Co(1)–O(13)^1	173.19(10)	O(11)–Co(2)–O(13)^3	88.85(10)	O(4)–Co(3)–O(5)	91.63(9)
O(10)–Co(1)–O(14)	95.24(9)	O(11)–Co(2)–N(3)	96.14(13)	O(4)^4–Co(3)–O(5)	170.79(9)
O(10)–Co(1)–O(14)^2	96.13(9)	O(14)–Co(2)–O(8)^3	107.84(10)	O(4)^4–Co(3)–N(6)	94.47(10)
O(10)–Co(1)–N(2)	88.55(12)	O(14)–Co(2)–O(11)	112.41(9)	O(4)–Co(3)–N(6)	173.71(10)
O(13)^1–Co(1)–O(9)^1	88.52(9)	O(14)–Co(2)–O(13)^3	80.15(9)	N(6)–Co(3)–O(5)	94.50(10)
O(13)^1–Co(1)–O(14)^2	81.14(9)	O(14)–Co(2)–N(3)	100.77(13)	O(4)–Co(4)–O(3)^1	81.54(8)
O(13)^1–Co(1)–N(2)	94.20(11)	N(3)–Co(2)–O(13)^3	174.08(12)	O(4)–Co(4)–O(6)	104.43(9)
O(14)^2–Co(1)–O(9)^1	89.94(9)	O(1)–Co(3)–O(3)^1	169.48(9)	O(4)–Co(4)–O(7)^4	114.08(9)
O(14)–Co(1)–O(9)^1	171.15(10)	O(1)–Co(3)–O(4)	94.43(9)	O(4)–Co(4)–N(8)^4	103.58(11)
O(14)–Co(1)–O(13)^1	90.53(8)	O(1)–Co(3)–O(4)^4	97.66(9)	O(6)–Co(4)–O(3)^1	84.77(9)
O(14)–Co(1)–O(14)^2	81.22(9)	O(1)–Co(3)–O(5)	84.82(9)	O(6)–Co(4)–O(7)^4	139.00(10)
O(14)–Co(1)–N(2)	98.42(11)	O(1)–Co(3)–N(6)	87.54(10)	O(6)–Co(4)–N(8)^4	94.13(11)
N(2)–Co(1)–O(9)^1	90.42(12)	O(3)^1–Co(3)–O(4)	82.49(8)	O(7)^4–Co(4)–O(3)^1	87.36(9)
N(2)–Co(1)–O(14)^2	175.32(11)	O(3)^1–Co(3)–O(5)	85.22(9)	O(7)^4–Co(4)–N(8)^4	90.21(11)
O(8)^3–Co(2)–O(13)^3	83.74(10)	O(3)^1–Co(3)–N(6)	96.60(10)	N(8)^4–Co(4)–O(3)^1	174.87(10)
O(8)^3–Co(2)–N(3)	90.43(14)	O(4)^4–Co(3)–O(3)^1	91.67(8)		

Symmetry codes: ^{1}–1+*x*, *y*, *z*; ^{2}–1–*x*, 1–*y*, 2–*z*; ^{3}–*x*, 1–*y*, 2–*z*; ^{4}–*x*, 2–*y*, 1–*z*; ^{5}1–*x*, 2–*y*, 1–*z*

CP **2**

Bond	Dist.	Bond	Dist.	Bond	Dist.
Co(1)–O(1)	2.0004(17)	Co(1)–N(5)^3	2.049(2)	Co(2)–O(4)^6	2.0840(17)
Co(1)–O(7)	1.9632(16)	Co(2)–O(7)	2.0617(16)	Co(2)–O(2)	2.0744(18)
Co(1)–O(4)^1	2.2526(17)	Co(2)–O(7)^4	2.1113(17)	Co(2)–N(2)	2.099(2)
Co(1)–O(6)^2	1.9990(18)	Co(2)–O(5)^5	2.1373(17)		
Angle	(°)	Angle	(°)	Angle	(°)
O(1)–Co(1)–O(4)^1	89.82(7)	N(5)^2–Co(1)–O(4)^1	177.80(8)	O(4)^6–Co(2)–O(5)^5	87.00(7)
O(1)–Co(1)–N(5)^2	90.29(9)	O(7)–Co(2)–O(7)^4	82.59(7)	O(4)^6–Co(2)–N(2)	95.36(8)
O(7)–Co(1)–O(1)	113.73(7)	O(7)^4–Co(2)–O(5)^5	89.51(7)	O(2)–Co(2)–O(7)^4	95.66(7)
O(7)–Co(1)–O(4)^1	79.82(6)	O(7)–Co(2)–O(5)^5	172.01(7)	O(2)–Co(2)–O(5)^5	85.81(7)
O(7)–Co(1)–O(6)^3	107.05(7)	O(7)–Co(2)–O(4)^6	90.46(6)	O(2)–Co(2)–O(4)^6	171.93(7)
O(7)–Co(1)–N(5)^2	102.14(9)	O(7)–Co(2)–O(2)	96.18(6)	O(2)–Co(2)–N(2)	88.01(8)
O(6)^3–Co(1)–O(1)	136.89(8)	O(7)–Co(2)–N(2)	99.98(8)	N(2)–Co(2)–O(7)^4	175.29(8)
O(6)^3–Co(1)–O(4)^1	83.99(7)	O(4)^6–Co(2)–O(7)^4	80.62(6)	N(2)–Co(2)–O(5)^5	87.81(8)
O(6)^3–Co(1)–N(5)^2	94.44(9)				

Symmetry codes: ^{1}1–*x*, 1–*y*, –*z*; ^{2}1/2+*x*, 1/2–*y*, –1/2+*z*; ^{3}3/2–*x*, 1/2+*y*, 1/2–*z*; ^{4}1–*x*, –*y*, –*z*; ^{5}1/2–*x*, –1/2+*y*, 1/2–*z*; ^{6}+*x*, –1+*y*, *z*; ^{7}–1/2+*x*, –1/2–*y* , –1/2+*z*

3 RESULTS AND DISCUSSION

3. 1 Crystal structure descriptions

3. 1. 1 Crystal structure of $\{[Co_8(DCPN)_4(1,2\text{-bimb})_4(\mu_3\text{-}OH)_4]\cdot(CH_3CN)_{0.5}(H_2O)_2\}_n$ (1)

Single-crystal X-ray diffraction analysis shows that **1** crystallizes in the triclinic system of $P\bar{1}$ space group. The asymmetric unit includes eight Co(II) ions, four $DCPN^{3-}$ ligands, four 1,2-bimb ligands, four coordinated μ_3-OH ions, a half of lattice acetonitrile molecule, and two lattice water molecules. As exhibited in Fig. 1a, Co(1)(II) is hexa-coordinated and encircled by three oxygen atoms (O(9A), O(10) and O(13A)) from two different $DCPN^{3-}$ ligands, two oxygen atoms (O(14) and O(14B)) from two μ_3-OH ions, and one nitrogen atom (N(2)) from one 1,2-bimb ligand, presenting a distorted octahedral geometry, while Co(2)(II) is penta-coordinated and connected by three oxygen atoms (O(8C), O(11) and O(13C)) from three different $DCPN^{3-}$ ligands, one oxygen atom (O(14)) from one μ_3-OH ion and one nitrogen atom (N(3)) from one 1,2-bimb ligand, giving a slightly distorted pyramidal geometry. As can be seen from Fig. 1b, two Co(1)(II) and two Co(2)(II) ions are connected by carboxylate oxygen atoms and μ_3-OH ions to form a tetranuclear $[Co_4(DCPN)_2(\mu_3\text{-}OH)_2]$ SBU with the shape of a parallelogram. The distances between the cobalt ions are 3.4384(8) and 3.0858(6) Å, respectively, and the bond angle of Co(2)–Co(1)–Co(2B) is 121.893(19)°.

Similar to the coordination mode of Co(1)(II) ion, Co(3)(II) ion also adopts a six-coordinate mode and is surrounded by three oxygen atoms (O(1), O(3A) and O(5)) from two different $DCPN^{3-}$ ligands, two oxygen atoms (O(4) and O(4D)) from two μ_3-OH ions and one nitrogen atom (N(6)) from one 1,2-bimb ligand, exhibiting a slightly distorted octahedral geometry, while Co(4) and Co(2) ions have similar coordination patterns (Fig. 1a). The Co(4)(II) ion displays a slightly distorted tetrahedral geometry, and is surrounded by three oxygen atoms (O(3A), O(6) and O(7D)) from three different $DCPN^{3-}$ ligands, one oxygen atom (O(4)) from one μ_3-OH ion and one nitrogen atom (N(8D)) from one 1,2-bimb ligand. Similarly, both carboxylate oxygen atoms and μ_3-OH ions connect with two Co(3)(II) and two Co(4)(II) ions to form another tetranuclear $[Co_4(DCPN)_2(\mu_3\text{-}OH)_2]$ SBU (Fig. 1c). The lengths of the adjacent cobalt ions are 3.3893(8) and 3.0838(7) Å, respectively, and the Co(4)–Co(3)–Co(4D) bond angle is 120.372(19)°. The bond lengths of Co–O and Co–N around all Co(II) ions fall in the 1.968(2)~2.266(2) Å and 2.065(3)~2.135(3) Å regions, respectively.

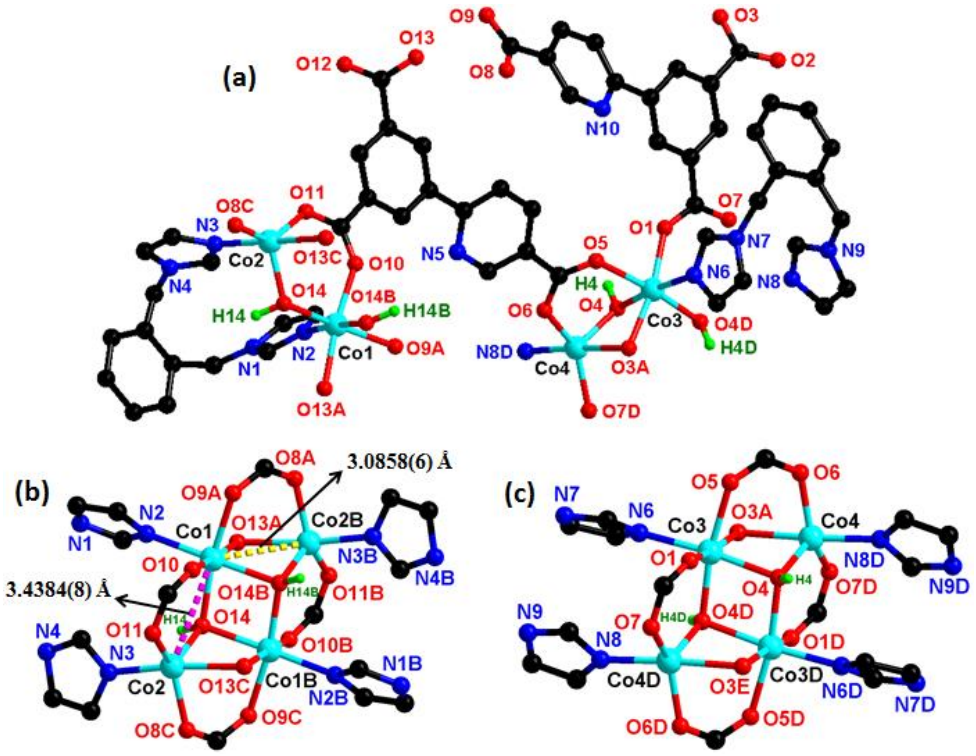

Fig. 1. (a) Coordination environment of 1; (b) Tetranuclear $[Co_4(DCPN)_2(\mu_3\text{-}OH)_2]$ SBU formed by Co(1) and Co(2) ions; (c) Tetranuclear $[Co_4(DCPN)_2(\mu_3\text{-}OH)_2]$ SBU formed by Co(3) and Co(4) ions.
Symmetry codes: A: –1+*x*, *y*, *z*; B: –1–*x*, 1–*y*, 2–*z*; C: –*x*, 1–*y*, 2–*z*; D: –*x*, 2–*y*, 1–*z*; E: 1–*x*, 2–*y*, 1–*z*

Three carboxylate groups of $DCPN^{3-}$ ligands are all deprotonated and adopted two different coordination modes: bridging bidentate (μ_2-η_1:η_1) and bridging unidentate (μ_2-η_2), which are also consistent with results of IR spectra (Fig. S1). Furthermore, the adjacent different tetranuclear [$Co_4(DCPN)_2(\mu_3\text{-}OH)_2$] SBUs are linked by the $DCPN^{3-}$ ligands to construct a 2D structure (Fig. 2a), in which the imidazole-N in 1,2-bimb ligands also coordinates with the Co(II) ion to further strengthen the 2D structure, as shown in Fig. 2b. The layered structure forms a 3D supramolecular framework through hydrogen bonding and π-π interactions (Fig. S3).

By TOPOs software, the framework of **1** is simplified as a (3,6)-c network with the point symbol of $(4^3)_2(4^6.6^6.8^3)$, when the $DCPN^{3-}$ ligands and tetranuclear [$Co_4(DCPN)_2(\mu_3\text{-}OH)_2$] SBUs are served as 3-c and 6-c nodes, respectively (Fig. 2c).

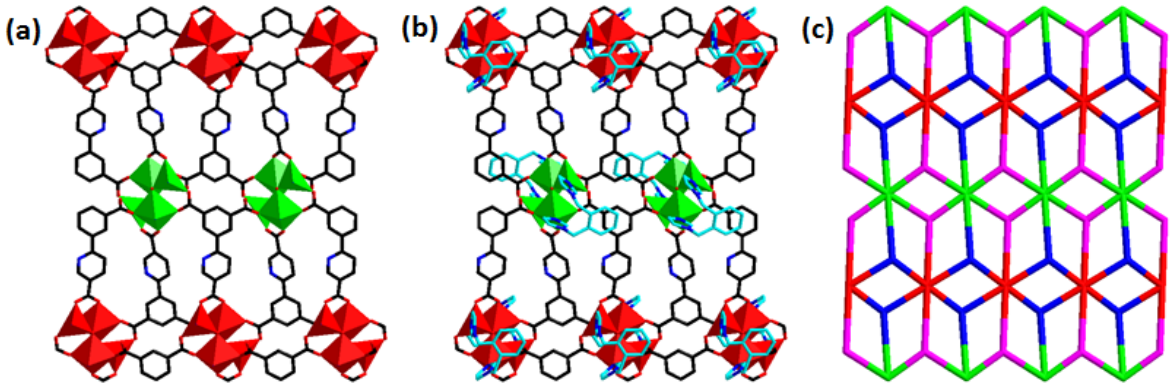

Fig. 2. (a) 2D structure of 1 based on Co(II) ions and $DCPN^{3-}$ ligands; (b) 3D framework of 1; (c) Topology of 1

3. 1. 2 Crystal structure of {[Co_2(DCPN)(1,3-bimb)(μ_3-OH)] H_2O}$_n$ (2)

Structural analysis shows that **2** crystallizes in the monoclinic space group $P2_1/n$. There are two crystallographically independent Co(II) ions, one $DCPN^{3-}$ ligand, one 1,3-bimb ligand, one coordinated μ_3-OH ion, and one lattice H_2O molecule in the asymmetric unit. As illustrated in Fig. 3, Co(1)(II) ion is penta-coordinated by three oxygen atoms (O(1), O(4A) and O(6B)) from three bridging unidentate carboxylate groups, one oxygen atom (O(7)) from one μ_3-OH ion, and one nitrogen atom (N(5C)) from one 1,3-bimb, while Co(2)(II) ion is hexa-coordinated and surrounded by one oxygen atom (O(2)) from one bridging unidentate carboxylate group, two oxygen atoms (O(4F) and O(5E)) from one chelating bidentate carboxylate group, two oxygen atoms (O(7) and O(7D)) from two μ_3-OH ions and one nitrogen atom (N(2)) from one 1,3-bimb. The distances of Co(1)···Co(2) and Co(2)···Co(1D) are 3.3925(7) and 3.0983(6) Å, respectively, and the bond angle of Co(1)–Co(2)–Co(1D) is 122.445(15)°. The bond lengths and bond angles around Co(1)(II) and Co(2)(II) ions are 1.9632(16)~2.2526(17) Å and 79.82(6)~177.80(8)°, respectively.

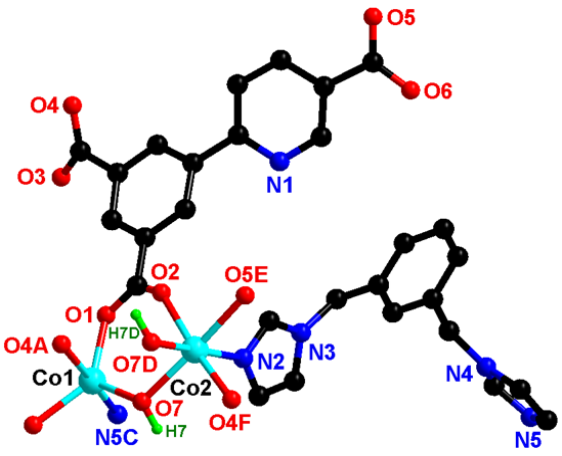

Fig. 3. Coordination environment of 2. Symmetry codes: A: 1–*x*, 1–*y*, –*z*; B: 1/2+*x*, 1/2–*y*, –1/2+*z*; C: 3/2–*x*, 1/2+*y*, 1/2–*z*; D: 1–*x*, –*y*, –*z*; E: 1/2–*x*, –1/2+*y*, 1/2–*z*; F: *x*, –1+*y*, *z*; G: –1/2+*x*, –1/2–*y*, –1/2+*z*

The coordination modes of carboxylate groups in $DCPN^{3-}$ ligand of **2** are the same as that in the $DCPN^{3-}$ ligand of **1**. As shown in Fig. 4a, two $DCPN^{3-}$ ligands and two μ_3-OH ions connect four Co(II) ions to form tetranuclear $[Co_4(DCPN)_2(\mu_3\text{-}OH)_2]$ SBU with the Co···Co separation of 3.39257(7) and 3.0983(6) Å, respectively, which are further expanded by $DCPN^{3-}$ ligands into a 2D layer structure (Fig. 4b).Then, the 2D layers are further connected with 1,3-bimb linkers to build a 3D network (Fig. 4c).

From the viewpoint of topology, if 1,3-bimb and $DCPN^{3-}$ ligands are respectively regarded as 2-c and 3-c nodes, and the tetranuclear $[Co_4(DCPN)_2(\mu_3\text{-}OH)_2]$ SBU is regarded as 10-c nodes, the 3D framework of **2** is simplified as a 3-nodal (2,3,10)-c 3D network with the point symbol of $\{4^3\}_2\{4^6.6^{16}.8^{21}.10^2\}\{6\}_2$ (Fig. 4d).

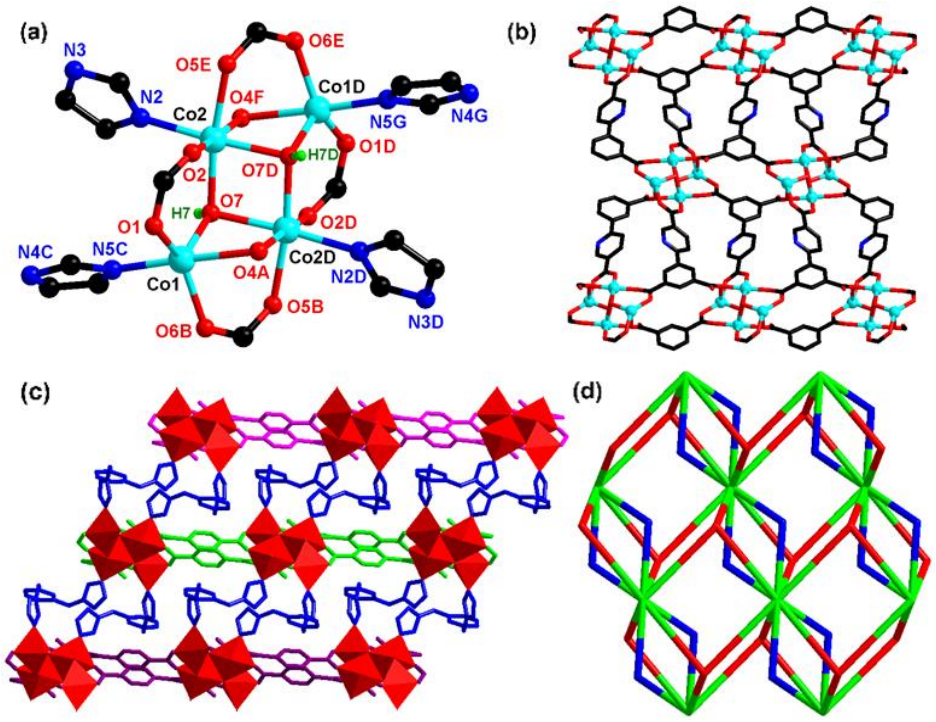

Fig. 4. (a) Tetranuclear $[Co_4(DCPN)_2(\mu_3\text{-}OH)_2]$ SBU formed by Co(II) ions; (b) 2D structure of 2 by Co(II) ions and $DCPN^{3-}$ ligands; (c) 3D framework of 2; (d) Topology of 2

3. 2 IR analyses, powder X-ray diffraction analyses and TGA analyses

As the IR spectra of **1** and **2** are similar (Fig. S1 and S2), **1** is taken as an example for detailed discussion. According to the IR spectra of **1**, the characteristic absorption peak at 3458 cm^{-1} is attributed to the stretching vibration peak of O–H bonds in the coordination OH^- ion and water molecule. The characteristic peak at 1529 cm^{-1} is attributed to the stretching vibration peak of C=N bonds in the H_3DCPN ligand and 1,2-bimb ligand. The two peaks of 1627 and 1440 cm^{-1} are attributed to antisymmetric stretching vibration and symmetric stretching vibration of the carboxylate groups H_3DCPN ligand, respectively, which has a separation of 187 cm^{-1} (< 200), indicating that the coordination mode of the carboxylate group in the formation of **1** is bidentate coordination[25]. Similarly, the corresponding data of the other group are 1606 and 1379 cm^{-1}, with a difference of 227 cm^{-1} (> 200), indicating monodentate coordination of the carboxylate group to the Co(II) ion. In conclusion, the carboxylate group in **1** adopts a mixed coordination mode, which is consistent with the analytical results of single crystal structure.

The phase purity of CPs was evaluated by X-ray powder diffraction, and the results showed that the main peaks of the synthesized samples are in good agreement with the simulated ones (Figs. S4 and S5), which indicates that the synthesized CPs have good phase purity. The difference in strength may be caused by the different orientation of the crystal powder.

In order to test the thermal stability of the two CPs, thermogravimetric analysis was performed from ambient temperature to 800 ℃ (Figs. S6 and S7). By analyzing the thermal weight loss curve of CP **1**, the weight loss of 2.23% below 300 ℃ is consistent with the lost two lattice water

molecules and half acetonitrile molecules (Found: 2.11%). The structure of **1** began to collapse at about 340 ℃. It can be seen from the thermal weight loss curve of CP **2** that the weight loss rate of 2.51% below 105 ℃ may correspond to the loss of one lattice water molecule (Found: 2.67%). The structure of **2** began to collapse above 350 ℃. The results showed that the total collapse temperature of the two CPs structures is over 340 ℃, showing both CPs have high thermal stability, which is very important for the practical application of CPs as functional materials.

3. 3 Magnetic properties

In order to study the magnetic properties of CPs, the temperature dependent magnetic susceptibilities χ_M of **1** and **2** under a constant magnetic field of 1000 Oe were measured in temperature range from 2 to 300 K. As exhibited in Fig. S8 and S9, CP **1** has no obvious magnetic phase transition, while CP **2** has a magnetic phase transition in the range of 20~40 K. The curves of $\chi_M T$ and χ_M^{-1} *vs T* are shown in Fig. 5. For **1**, the χ_MT experimental value of 9.89 cm^3 K mol^{-1} at room temperature is higher than that of four spin-only Co(II) ions (7.50 cm^3 K mol^{-1}, S = 3/2, g = 2.0), which may be attributed to the formation of unquenched orbital moment caused by the spin-orbit coupling in the distorted octahedral coordination of Co(II) ion[26, 27]. As shown in Fig. 5a, the $\chi_M T$ value decreased monotonously with the decrease of temperature, finally reached the minimum value of 0.21 at 2.0 K. The result at high temperature region reveals the antiferromagnetic interaction between neighboring Co(II) ions in CP **1**[26]. The decrease of the $\chi_M T$ value at low temperature can be due to the contribution of the orbital momentum of the single Co(II) ion, intermolecular antiferromagnetic coupling interaction, and intramolecular antiferromagnetic coupling interaction between neighboring Co(II) ions[28-30]. In addition, the curve of χ_M^{-1} *vs* T is not completely linear. In the range of 40~300 K, the magnetic susceptibility is fitted according to the Curie-Weiss law (χ_M = C/(T–θ)), with the Curie constant C of 17.61 cm^3 K mol^{-1} and the Weis constant θ of –241.95 K, which is confirmed again the antiferromagnetic interaction exhibited in **1**.

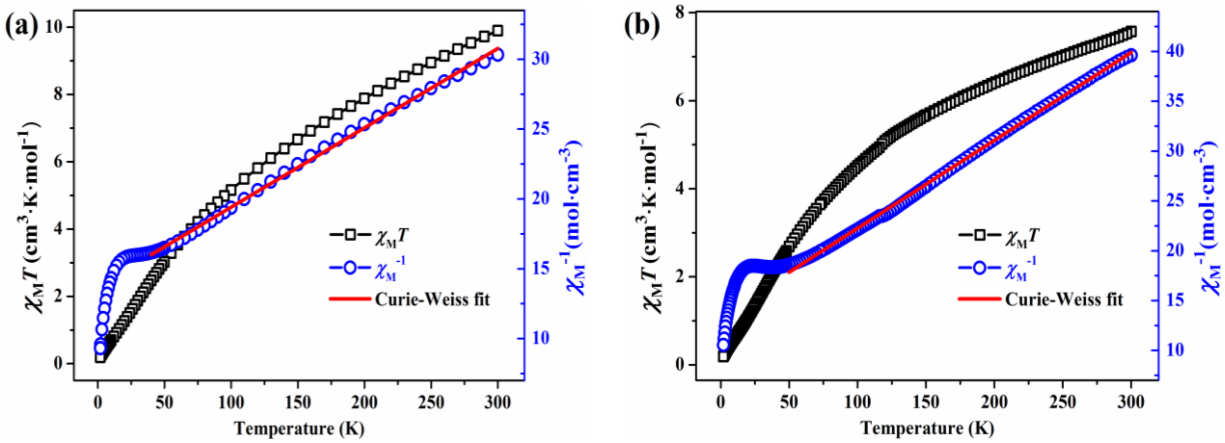

Fig. 5. Temperature dependence of magnetic susceptibilities of 1(a) and 2(b) under a static field of 1000 Oe

As for **2**, the $\chi_M T$ value of 7.57 cm^3 K mol^{-1} at 300 K is close to the calculated value of 7.50 cm^3 K mol^{-1} for four isolated high-spin Co(II) ions. As shown in Fig. 5b, the $\chi_M T$ value decreased monotonously with the continuous decrease of temperature and reached the minimum value of 0.19 cm^3 K mol^{-1} at 2 K. Similar to **1**, the magnetic susceptibilities obey the Curie-Weiss law in the temperature range above 50 K for **2**, giving a negative Weiss constant θ = –152.25 K and Curie constant C = 11.34 cm^3 K mol^{-1} for **2**, respectively. According to the variation trend of $\chi_M T$ value and the negative Weiss constant, the antiferromagnetic interaction also exists between adjacent Co(II) ions in **2**.

The above magnetic difference between the two CPs is related to their structures. In these two CPs, H_3DCPN ligands have very similar coordination patterns. Although two different tetranuclear $Co_4(DCPN)_2(\mu_3\text{-}OH)_2$] SBUs are formed in **1**, they both form 2D layered structures when connected to the Co(II) ions. Interestingly, the introduction of imidazole ligands causes structural changes. Specifically, ligand 1,2-bimb is directly connected to Co(II) ions in the same SUB, so that **1** remains a 2D structure, while ligand 1,3-bimb molecules are connected to different SUB, so that different layered structures are connected to form 3D structures, thus resulting in their different properties.

4 CONCLUSION

In summary, two novel Co-based CPs have been solvothermally synthesized by the reaction of H_3DCPN, 1,2-bimb, 1,3-bimb and cobalt salts. Meanwhile, **1** and **2** have good phase purities and high thermal stability, while 1,2-bimb and 1,3-bimb bridging linker help form different structures in the self-assembly process of CPs. In addition, magnetic studies indicated that **1** and **2** both have antiferromagnetic interactions between the adjacent Co(II) ions.

REFERENCES

(1) Xue, D. X.; Wang, Q.; Bai, J. F. Amide-functionalized metal-organic frameworks: syntheses, structures and improved gas storage and separation properties. *Coord*. *Chem*. *Rev*. **2019**, 378, 2–16.

(2) Sun, Y. J.; Tan, Q. H.; Liu, X. L.; Gao, Y. F.; Zhang, J. Probing the magnetic ordering of antiferromagnetic $MnPS_3$ by Raman spectroscopy. *J*. *Phys*. *Chem. Lett*. **2019**, 10, 3087–3093.

(3) Zhang, Z. S.; Zhang, Y. X.; Luo, X. H.; Ma, S. C.; Zeng, H.; Yu, G.; Zheng, X. M.; Chen, C. C.; Hu, Y. F.; Xu, F.; Rehman, S. U.; Zhong, Z. C. Self-organized Bi-rich grain boundary precipitates for realizing steep magnetic-field-driven metamagnetic transition in Bi-doped Mn_2Sb. *Acta Mater*. **2020**, 200, 835–847.

(4) Chen, H. T.; Zhuang, G. L.; Fan, L. M.; Zhang, X. T.; Gao, L. N.; Sun, D. A highly robust heterometallic Tb^{III}/Ni^{II}-organic framework for C_2 hydrocarbon separation and capture. *Chem. Commun*. **2020**, 56, 2047–2050.

(5) Gao, W. Y.; Tsai, C. Y.; Wojtas, L.; Thiounn, T.; Lin, C. C.; Ma, S. Q. Interpenetrating metal-metalloporphyrin framework for selective CO_2 uptake and chemical transformation of CO_2. *Inorg*. *Chem*. **2016**, 55, 7291–7294.

(6) Zhang, W.; Wang, X.; Li, P.; Zhang, W.; Wang, H.; Tang, B. Evaluating hyperthyroidism-induced liver injury based on in situ fluorescence imaging of glutathione and phosphate via nano-MOFs sensor. *Anal*. *Chem*. **2020**, 92, 8952–8958.

(7) Wang, J. J.; Si, P. P.; Liu, M. J.; Chen, Y.; Yu, S. X.; Lu, M.; Wang, S. Y.; Li, B.; Li, P. P.; Zhang, R. C. Selective fluorescent sensing and photodegradation properties of Tb(III)-based MOFs with different bulky backbone ligands. *Polyhedron*. **2019**, 157, 63–70.

(8) Chen, D. P.; Luo, R.; Li, M. Y.; Wen, M. Q.; Li, Y.; Chen, C.; Zhang, N. Salen(Co(III)) imprisoned within pores of a metal-organic framework by post-synthetic modification and its asymmetric catalysis for CO_2 fixation at room temperature. *Chem. Commun*. **2017**, 53, 10930–10933.

(9) Han, W. G.; Huang, X. S.; Lu, G. X.; Tang, Z. C. Research progresses in the preparation of Co-based catalyst derived from Co-MOFs and application in the catalytic oxidation reaction. *Catal*. *Surv*. *Asia*. **2019**, 23, 64–89.

(10) Wu, C. M.; Tsai, J. E.; Lee, G. H.; Yang, E. C. Slow magnetization relaxation in a tetrahedrally coordinated mononuclear Co(II) complex exclusively ligated with phenanthroline ligands. *Dalton Trans*. **2020**, 49, 16813–16820.

(11) Ling, X. Y.; Wang, J.; Gong, C. H.; Lu, L.; Singh, A. K.; Kumar, A.; Sakiyama, H.; Yang, Q. Q.; Liu, J. Q. Modular construction, magnetism and photocatalytic properties of two new metal-organic frameworks based on a semi-rigid tetracarboxylate ligand. *J. Solid State Chem*. **2019**, 277, 673–679.

(12) Drahoš, B.; Šalitroš, I.; Císařová, I.; Herchel, R. A multifunctional magnetic material based on a solid solution of Fe(II)/Co(II) complexes with a macrocyclic cyclam-based ligand. *Dalton Trans*. **2021**, 50, 11147–11157.

(13) Li, Y.; Wu, J.; Gu, J. Z.; Qiu, W. D.; Feng, A. S. Temperature-dependent syntheses of two manganese(II) coordination compounds based on an ether-bridged tetracarbolylic acid. *Chinese*. *J*. *Struct*. *Chem*. **2020**, 39, 727–736.

(14) Pantazis, D. A.; Krewald, V.; Orio, M.; Neese, F. Theoretical magnetochemistry of dinuclear manganese complexes: broken symmetry density functional theory investigation on the influence of bridging motifs on structure and magnetism. *Dalton Trans*. **2010**, 39, 4959–4967.

(15) Han, B. L.; Liu, Z.; Feng, L.; Wang, Z.; Gupta, R. K.; Aikens, C. M.; Tung, C. H.; Sun, D. Polymorphism in atomically precise Cu_{23} nanocluster incorporating tetrahedral $[Cu_4]^0$ kernel. *J*. *Am*. *Chem*. *Soc*. **2020**, 142, 5834–5841.

(16) Wang, F.; Zhuo, H. Y.; Han, X. G.; Chen, W. M.; Sun, D. Foam-like CoO@N,S-codoped carbon composites derived from a well-designed N,S-rich Co-MOF for lithium-ion batteries. *J*. *Mater*. *Chem*. *A*. **2017**, 5, 22964–22969.

(17) Zenno, H.; Kobayashi, F.; Nakamura, M.; Sekine, Y.; Lindoy, L. F.; Hayami, S. Hydrogen bond-induced abrupt spin crossover behaviour in 1-D cobalt(II) complexes-the key role of solvate water molecules. *Dalton Trans*. **2021**, 50, 7843–7853.

(18) Wang, Z.; Liu, J. W.; Su, H. F.; Zhao, Q. Q.; Kurmoo, M.; Wang, X. P.; Tung, C. H.; Sun, D.; Zheng, L. S. Chalcogens-induced $Ag_6Z_4@Ag_{36}$ (Z=S or Se) core-shell nanoclusters: enlarged tetrahedral core and homochiral crystallization. *J*. *Am*. *Chem*. *Soc*. **2019**, 141, 17884–17890.

(19) Yang, Y.; Jia, T.; Han, Y. Z.; Nan, Z. A.; Yuan, S. F.; Yang, F. L.; Sun, D. An all-alkynyl protected 74-nuclei silver(I)-copper(I)-oxo nanocluster: oxo-induced hierarchical bimetal aggregation and anisotropic surface ligand orientation. *Angew Chem. Int. Ed*. **2019**, 58, 12280–12285.

(20) Mortazavi, B.; Shahrokhi, M.; Hussain, T.; Zhuang, X. Y. Theoretical realization of two-dimensional $M_3(C_6X_6)_2$ (M = Co, Cr, Cu, Fe, Mn, Ni, Pd, Rh and X = O, S, Se) metal-organic frameworks. *Appl. Mater. Today*. **2019**, 15, 405–415.

(21) Liu, J. W.; Feng, L.; Su, H. F.; Wang, Z.; Zhao, Q. Q.; Wang, X. P.; Tung, C. H.; Sun, D.; Zheng, L. S. Anisotropic assembly of Ag_{52} and Ag_{76} nanoclusters. *J. Am. Chem. Soc.* **2018**, 140, 1600–1603.

(22) Dolomanov, O. V.; Bourhis, L. J.; Gildea, R. J.; Howard, J. A.; Puschmann, K. H. OLEX 2: a complete structure solution, refinement and analysis program. *J. Appl. Crystallogr*. **2009**, 42, 339–341.

(23) The network topology was evaluated by the program"TOPOS-4.0" see: http://www.topos.ssu.samara.ru.

(24) Blatow, V. A. Nanocluster analysis of intermetallic structures with the program package TOPOS. *Struct. Chem.* **2012**, 23, 955–963.

(25) Ma, X. W.; Dong, J.; Zhang, J. X.; Wu, W. F.; Ran, H.; Zhang, P. Y. Two novel metal coordination polymers: anticancer activity in human angioneoplasm cells. *Chinese. J. Struct. Chem.* **2019**, 7, 1146–1151.

(26) Wang, H.; Zhang, D.; Sun, D.; Chen, Y.; Zhang, L. F.; Tian, L.; Jiang, J.; Ni, Z. H. Co(II) metal-organic frameworks (MOFs) assembled from asymmetric semirigid multicarboxylate ligands: synthesis, crystal structures, and magnetic properties. *Cryst. Growth. Des.* **2009**, 9, 5273–5282.

(27) Chen, Z. L.; Li, Y.; Jiang, C. F.; Liang, F. P.; Song, Y. Metal complexes with N-(2-pyridylmethyl)iminodiacetate: from discrete polynuclear compounds to 1D coordination polymers. *Dalton Trans.* **2009**, 27, 5290–5299.

(28) Liu, T.; Huang, Y. M.; Zou, H. H.; Wang, H. L.; Liang, F. P. Synthesis, structural characterization and magnetocaloric effect of a butterfly $[Co^{II}_2Gd^{III}_2]$ cluster. *Chinese. J. Struct. Chem.* **2019**, 38, 1152–1158.

(29) Hu, X. X.; Xu, J. Q.; Cheng, P.; Chen, X. Y.; Cui, X. B.; Song, J. F.; Yang, G. D.; Wang, T. G. A new route for preparing coordination polymers from hydrothermal reactions involving in situ ligand synthesis. *Inorg. Chem.* **2004**, 43, 2261–2266.

(30) Wang, C. C.; Tsai, J. H.; Ke, S. Y.; Lee, G. H.; Chuang, Y. C.; Yang, E. C. Structural characterization, water adsorption, and magnetic properties of two composite Mn(II)-squarate-dpe supramolecular architectures. *Cryst. Growth Des.* **2020**, 20, 5395–5405.